Two-color ghost imaging

Kam Wai Clifford Chan,* Malcolm N. O'Sullivan,† and Robert W. Boyd‡
The Institute of Optics, University of Rochester, Rochester, New York 14627, USA
(Received 10 September 2008; published 9 March 2009)

Nondegenerate-wavelength (or two-color) ghost imaging using either thermal or quantum light sources is studied theoretically. We demonstrate that a high-quality ghost image can be obtained even when the wavelengths of light used in the object and reference arms are very different. The spatial resolution of the ghost image is found in general to depend on each of these wavelengths, although in many practical situations it depends primarily on the wavelength used to illuminate the object. The resolution of nondegenerate-wavelength thermal ghost imaging can be higher than that of its quantum counterpart despite the fact that the photons have the same degree of spatial correlation in the two cases.

DOI: 10.1103/PhysRevA.79.033808 PACS number(s): 42.30.Va, 42.50.Ar

I. INTRODUCTION

Ghost imaging is an indirect imaging method that acquires the image of an object through spatial intensity correlation measurements. In the imaging setup, two spatially correlated light fields are used: an object field that illuminates the object but is not spatially resolved by its detector and a reference field that does not interact with the object but is spatially resolved by its detector. Then, by measuring the intensity cross-correlation function of the object and reference fields, an image (the "ghost image") can be obtained. By separating the process of forming the image from that of interrogating the object, new possibilities for enhanced image formation and remote sensing are made possible.

The correlation that leads to ghost imaging can be of a quantum or classical nature. Quantum ghost imaging utilizes the spatial entanglement of biphotons generated, for instance, by spontaneous parametric down conversion (SPDC) [1], whereas thermal ghost imaging (sometimes called classical ghost imaging) is achieved by using two exact copies of spatially incoherent light [2–4]. We stress that within this paper we use the terms quantum and thermal in the sense defined in the previous sentence. We note that other authors at times use these terms to mean somewhat different things. For instance the authors in Ref. [5] have presented arguments that even thermal ghost imaging displays quantum features, whereas those in Ref. [6] have pointed out that many features of ghost imaging based on parametric down conversion (PDC) can be understood classically. More interestingly, the authors in Ref. [7] suggest that the quantum nature of the light source can be tuned between the entangled and separable regimes while the possibility of realizing ghost imaging is not affected. Furthermore, a distinction can be drawn as to whether the correlations that lead to ghost imaging are of a phase-sensitive or a phase-insensitive nature [6]. As the primary intent of this paper is to explore the utility of two-color ghost imaging, we will simply use our terminology as an operational way of explaining what type of ghost imaging we are considering.

*kwchan@optics.rochester.edu
†osulliva@optics.rochester.edu
‡boyd@optics.rochester.edu

The object and reference fields used in ghost imaging need not have the same wavelength. Indeed, nondegenerate-wavelength quantum ghost imaging has already been demonstrated experimentally [8], although thermal ghost imaging experiments have been carried out only for the single-frequency situation. It is natural to ask how the spatial resolution of the ghost image depends on each of the wavelengths that is used. The wavelength dependence of the resolution has been studied in detail for the degenerate-wavelength ghost imaging [6,9] and the nondegenerate-wavelength quantum ghost imaging with a plane-wave pump field [10].

In this paper, we demonstrate theoretically that nondegenerate-wavelength ghost imaging can be carried out using either classical or quantum correlations. We obtain analytical results which show that the resolution of nondegenerate-wavelength ghost imaging depends primarily on the wavelength of the light that illuminates the object, although more generally it depends also on the wavelength of the light in the reference arm. For thermal ghost imaging, the light beams in the object and reference arms can have very different wavelengths, whereas for quantum ghost imaging the crystal properties often impose a limit on how different the signal and idler wavelengths can be. Moreover, we find that the image resolution for the classical scheme can be higher than that for its quantum counterpart despite the fact that the photons have the same degree of spatial correlation in the two schemes. These results are potentially important for cases in which the optimal wavelength of light that illuminates the object is very different from the optimal wavelength for the operation of the spatially resolving detector. Finally we compare our results with those presented in Ref. [10].

II. THEORY OF TWO-COLOR GHOST IMAGING

To study the properties of nondegenerate-wavelength ghost imaging, we consider the setups depicted in Fig. 1. The setup for thermal ghost imaging is shown in Fig. 1(a) and the corresponding quantum ghost imaging setup is shown in Fig. 1(b). An object with amplitude transmission function $O(\vec{x}_o'')$ is placed in the object arm. The lens in the reference arm is a necessary component for the quantum ghost imaging setup

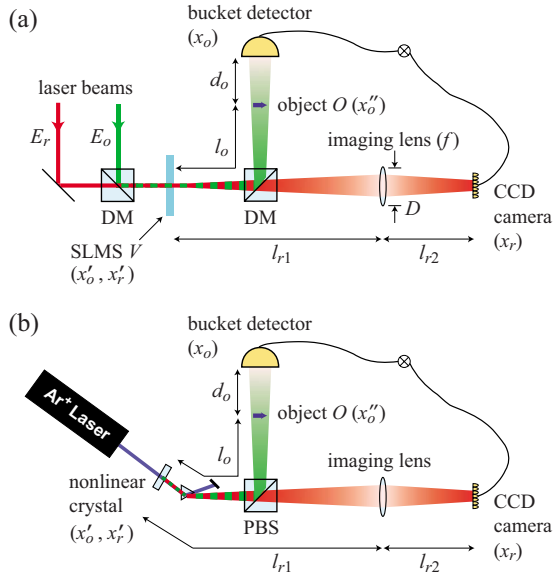

FIG. 1. (Color online) (a) Setup for nondegenerate-wavelength thermal ghost imaging. Identical random intensity patterns are impressed onto two laser beams of wavelengths λ_o and λ_r by passing them through the same spatial light modulating system (SLMS). One of the beams is then used to illuminate the object and the transmitted power is measured by a bucket detector. The transverse intensity distribution of the other beam, known as the reference beam, is measured by an imaging detector such as a charge coupled device (CCD) camera. The correlation signal between the outputs of the two detectors produces the "ghost" image of the object. (b) The corresponding setup for nondegenerate-wavelength quantum ghost imaging. Here, correlations between the two beams are created by the process of PDC. DM: dichroic mirror; PBS: polarizing beam splitter.

but is optional for the classical scheme [5,11,12] for reasons that we explain below.

For thermal ghost imaging, two laser beams with central frequencies Ω_o and Ω_r are made to coincide and pass through some SLMS that impresses the same spatial intensity pattern onto each beam. In degenerate-wavelength thermal ghost imaging, typically a rotating ground glass plate followed by a beam splitter is used to create two correlated copies of the spatially incoherent light beams. However, in nondegenerate-wavelength thermal ghost imaging, this method is not suitable for creating spatial correlations between the two laser beams, as the phase shifts imposed on them by the ground glass plate can be very different when Ω_o is substantially different from Ω_r. One possible means for producing spatial correlations between the beams is to use an amplitude mask that generates random spatial patterns following Gaussian statistics. In this way, the two light fields are rendered spatially incoherent but in a correlated fashion. For the quantum case, entangled signal and idler photons generated by SPDC are used in the object and reference arms, respectively.

Let us consider in detail the analysis of nondegenerate-wavelength thermal ghost imaging. The fields arriving at the bucket detector in the object arm and at the CCD camera in the reference arm can be expressed as

$$E_a(\vec{x}_a,t) = \int d\omega d\vec{q} e^{-i\omega t} V(\vec{q}) \mathcal{E}_a(\omega) H_a(\vec{x}_a,\vec{q};\omega), \qquad (1)$$

where the laser fields incident on the SLMS are taken to be plane waves with spectra $\mathcal{E}_a(\omega)$, where $a=o,r$. The SLMS produces spatial amplitude modulation of the light fields represented by the random spatial mask function $V(\vec{q})$, which is taken to be the same for both ω_o and ω_r. The functions H_o and H_r are transfer functions that describe propagation through the object and reference arms with the object transmission function $O(\vec{x}_o'')$ incorporated into H_o. The quantities $\vec{x}$ and $\vec{q}$ represent transverse position and wave vector. The ghost image is obtained from the intensity cross-correlation function. For later convenience we subtract the background signal, which comes from the average intensities of light received by the bucket detector and the CCD camera, from the intensity cross-correlation function. We thus obtain

$$\begin{aligned} C(\vec{x}_o,\vec{x}_r,t) &\equiv \langle |E_o(\vec{x}_o,t)|^2 |E_r(\vec{x}_r,t)|^2 \rangle - \langle |E_o(\vec{x}_o,t)|^2 \rangle \langle |E_r(\vec{x}_r,t)|^2 \rangle \\ &= \int d\omega_o d\omega_o' d\vec{q}_o d\vec{q}_o' d\omega_r d\omega_r' d\vec{q}_r d\vec{q}_r' H_o^*(\vec{x}_o,\vec{q}_o;\omega_o) H_o(\vec{x}_o,\vec{q}_o';\omega_o') H_r^*(\vec{x}_r,\vec{q}_r;\omega_r) H_r(\vec{x}_r,\vec{q}_r';\omega_r') e^{i(\omega_o-\omega_o')t} e^{i(\omega_r-\omega_r')t} \\ &\quad \times G(\vec{q}_o,\vec{q}_o',\vec{q}_r,\vec{q}_r',\omega_o,\omega_o',\omega_r,\omega_r'), \end{aligned} \qquad (2)$$

where

$$\begin{aligned} G(\vec{q}_o,\vec{q}_o',\vec{q}_r,\vec{q}_r',\omega_o,\omega_o',\omega_r,\omega_r') &= \langle V^*(\vec{q}_o) V(\vec{q}_o') V^*(\vec{q}_r) V(\vec{q}_r') \rangle \langle \mathcal{E}_o^*(\omega_o) \mathcal{E}_o(\omega_o') \mathcal{E}_r^*(\omega_r) \mathcal{E}_r(\omega_r') \rangle - \langle V^*(\vec{q}_o) V(\vec{q}_o') \rangle \langle V^*(\vec{q}_r) V(\vec{q}_r') \rangle \\ &\quad \times \langle \mathcal{E}_o^*(\omega_o) \mathcal{E}_o(\omega_o') \rangle \langle \mathcal{E}_r^*(\omega_r) \mathcal{E}_r(\omega_r') \rangle \end{aligned} \qquad (3)$$

is the intensity cross-correlation function of the light beams in the spatial and temporal frequency domain evaluated at the output surface of the SLMS.

The fields $\mathcal{E}_o$ and $\mathcal{E}_r$ are taken to be two independent quasimonochromatic light fields with central frequencies of Ω_o and Ω_r. In addition, the SLMS mask function V is taken

to possess spatial correlations that follow Gaussian statistics. In this way, Eq. (3) becomes

$$G(\vec{q}_o,\vec{q}_o',\vec{q}_r,\vec{q}_r',\omega_o,\omega_o',\omega_r,\omega_r') = \langle V^*(\vec{q}_o)V(\vec{q}_r')\rangle\langle V^*(\vec{q}_r)V(\vec{q}_o')\rangle \times\langle\mathcal{E}_o^*(\omega_o)\mathcal{E}_o(\omega_o')\rangle \times\langle\mathcal{E}_r^*(\omega_r)\mathcal{E}_r(\omega_r')\rangle, \quad (4)$$

and we can thus write the correlation function of Eq. (2) as

$$C(\vec{x}_o,\vec{x}_r) = B\left|\int d\vec{x}_o' d\vec{x}_r' W(\vec{x}_o',\vec{x}_r')H_o(\vec{x}_o,\vec{x}_o';\Omega_o)H_r^*(\vec{x}_r,\vec{x}_r';\Omega_r)\right|^2, \quad (5)$$

where $B=I_oI_r$ with $I_a=\langle|\int d\omega_a\mathcal{E}_a(\omega_a)e^{-i\omega_a t}|^2\rangle$ being the product of the average intensities of the two beams of the light incident on the SLMS. Also, $W(\vec{x}_o',\vec{x}_r')$ is the spatial Fourier transform of $\langle V(\vec{q}_o')V^*(\vec{q}_r')\rangle$, and the transfer functions H_o and H_r are written in position space. The quantity $W(\vec{x}_o',\vec{x}_r')$ can be interpreted as the spatial cross-correlation function of the light fields in the plane of the SLMS. The correlation arises from the random amplitude mask that renders the individual light beams spatially incoherent but with the same intensity profile, as described by Eq. (1). From Eq. (5), we see that the correlation function $C(\vec{x}_o,\vec{x}_r)$ has the same form as that for degenerate-wavelength ghost imaging [3]. Therefore, nondegenerate-wavelength thermal ghost imaging is possible even when the difference of the wavelengths is very large, provided that a suitable SLMS is used to create the same spatial modulations for the two beams of light.

We can treat the case of nondegenerate-wavelength quantum ghost imaging using an analogous formalism. In the narrow-bandwidth limit, the coincidence count rate for the quantum ghost imaging takes a form similar to Eq. (5), except that the transfer function H_r is not conjugated and the spatial correlation function $W(\vec{x}_o',\vec{x}_r')$ is replaced by the two-photon wave function $\psi(\vec{x}_o',\vec{x}_r')$ at the output surface of the nonlinear crystal [8,13]. Typically, the biphoton wave function for photons produced by SPDC takes a form similar to that of $W(\vec{x}_o',\vec{x}_r')$, which is defined for thermal light. Thus, for example, the entanglement area of a biphoton is related to the spatial correlation area of thermal light. We can thereby apply the analysis for thermal ghost imaging to the quantum case by simply replacing Ω_o with $-\Omega_o$ [4,12,14].

III. INTERPRETATION IN TERMS OF COHERENCE PROPAGATION

For the ghost imaging setup in Fig. 1, the transfer functions are given by

$$H_o(\vec{x}_o,\vec{x}_o') = \int d\vec{x}_o'' h_0(\vec{x}_o,\vec{x}_o'';\lambda_o d_o)O(\vec{x}_o'')h_0(\vec{x}_o'',\vec{x}_o';\lambda_o l_o), \quad (6)$$

and

$$H_r(\vec{x}_r,\vec{x}_r') = \int d\vec{\xi}_r h_0(\vec{x}_r,\vec{\xi}_r;\lambda_r l_{r2})L(\vec{\xi}_r)h_0(\vec{\xi}_r,\vec{x}_r';\lambda_r l_{r1}), \quad (7)$$

where $h_0(\vec{x},\vec{x}';z)=(iz)^{-1}\exp[i(\pi/z)(\vec{x}-\vec{x}')^2]$ is the paraxial free-space propagator, $L(\vec{x})=\exp[-i\pi/(\lambda_r f)\vec{x}^2]\Theta(|\vec{x}|-D)$ is the transmission function of the imaging lens with focal length f and aperture radius D, and $\Theta(x)$ is the unit step function. By assumption, the bucket detector does not provide spatial resolution, and thus to determine the form of the ghost image, we integrate $C(\vec{x}_o,\vec{x}_r)$ over all $\vec{x}_o$, that is, over the surface area of the bucket detector. Using Eqs. (5)–(7), we thereby obtain a quantity of the form

$$P(\vec{x}_r) \equiv \int d\vec{x}_o C(\vec{x}_o,\vec{x}_r) = B\int d\vec{x}_o''|O(\vec{x}_o'')|^2 \times\left|\int d\vec{x}_o' d\vec{x}_r' W(\vec{x}_o',\vec{x}_r')h_0(\vec{x}_o'',\vec{x}_o';\lambda_o l_o)H_r^*(\vec{x}_r,\vec{x}_r')\right|^2. \quad (8)$$

This quantity, $P(\vec{x}_r)$, gives the power distribution of the ghost image. Note that $P(\vec{x}_r)$ depends on the object intensity transmittance function $O(\vec{x}_o'')$. We shall see below that under suitable conditions $P(\vec{x}_r)$ is a faithful representation of the object transmittance.

Equation (8) can be put into a more suggestive form if we write Eq. (7) as

$$H_r(\vec{x}_r,\vec{x}_r') = \int d\vec{x}_r''\tilde{H}_r(\vec{x}_r,\vec{x}_r'')h_0(\vec{x}_r'',\vec{x}_r';\lambda_o l_o), \quad (9)$$

where

$$\tilde{H}_r(\vec{x}_r,\vec{x}_r'') = \int d\vec{\xi}_r h_0(\vec{x}_r,\vec{\xi}_r;\lambda_r l_{r2})L(\vec{\xi}_r)h_0(\vec{\xi}_r,\vec{x}_r'';\lambda_r l_{r1}-\lambda_o l_o) \quad (10)$$

represents the propagation from an effective object plane (see the discussion below) to the CCD through the imaging lens. We then define the quantity

$$\tilde{W}(\vec{x}_o'',\vec{x}_r'') = \int d\vec{x}_o' d\vec{x}_r' W(\vec{x}_o',\vec{x}_r')h_0(\vec{x}_o'',\vec{x}_o';\lambda_o l_o)h_0^*(\vec{x}_r'',\vec{x}_r';\lambda_o l_o). \quad (11)$$

In terms of this quantity, the expression for the ghost image takes the form

$$P(\vec{x}_r) = B\int d\vec{x}_o''\left|O(\vec{x}_o'')\int d\vec{x}_r''\tilde{W}(\vec{x}_o'',\vec{x}_r'')\tilde{H}_r^*(\vec{x}_r,\vec{x}_r'')\right|^2. \quad (12)$$

The function $\tilde{W}(\vec{x}_o'',\vec{x}_r'')$ of Eq. (11) is the coherence function $W(\vec{x}_o',\vec{x}_r')$ propagated through a free-space distance l_o at wavelength λ_o onto the object plane $(\vec{x}_o'')$ and a distance $(\lambda_o/\lambda_r)l_o$ at wavelength λ_r onto the effective object plane $(\vec{x}_r'')$. The effective object plane is the surface that has the same spatial intensity pattern at wavelength λ_r as the object plane at wavelength λ_o. This is illustrated in Fig. 2(a) as a ray diagram unfolded in the sense that the object and reference arms are drawn on the opposite sides of the light source. For thermal ghost imaging, the light source represents the

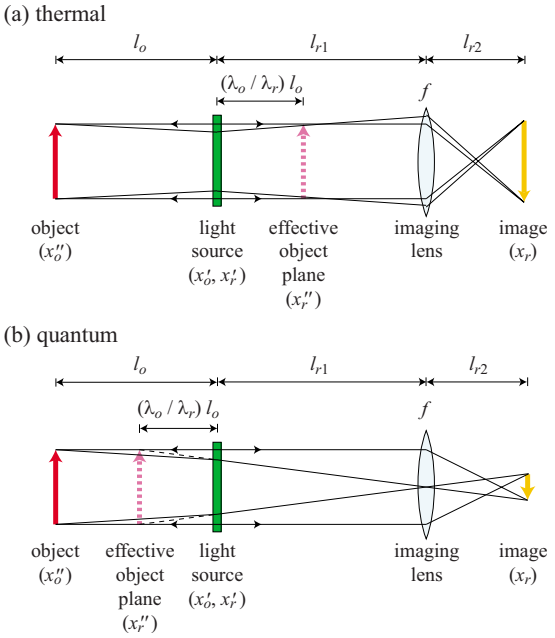

FIG. 2. (Color online) Unfolded ray diagrams used to describe ghost imaging. Both thermal and quantum ghost imaging entail imaging an effective object plane onto the image plane. The position of the effective object plane depends on both λ_o and λ_r. For definiteness the figure is drawn for the situation $\lambda_o < \lambda_r$.

output of the SLMS and the effective object plane is located on the side of the reference arm. This can be seen from Eq. (9), which manifests that the reference arm is partitioned into two parts separated by the effective object plane. The bucket detector collects all the light passing through the object, and the CCD camera in the reference arm works as if it were imaging a real image at the effective object plane. The transfer function $\tilde{H}_r(\vec{x}_r, \vec{x}_r'')$ describes the role of the imaging lens in relaying the field from the effective object plane to the CCD. Note that in the conventional Klyshko pictures, the image formation of ghost imaging is interpreted using geometric optics [1,4,14]. Here we obtain an equivalent picture by utilizing the description based on coherence propagation. The coherence propagation description of ghost imaging with Gaussian-state light is also treated in Ref. [6].

To treat the case of nondegenerate-wavelength quantum ghost imaging, we replace Eq. (10) by

$$\tilde{H}_r(\vec{x}_r, \vec{x}_r'') = \int d\vec{\xi}_r h_0(\vec{x}_r, \vec{\xi}_r; \lambda_r l_{r2}) L(\vec{\xi}_r) h_0(\vec{\xi}_r, \vec{x}_r''; \lambda_r l_{r1} + \lambda_o l_o). \tag{13}$$

Then we find the expression for the quantum ghost image to be

$$P(\vec{x}_r) = B \int d\vec{x}_o'' \left| O(\vec{x}_o'') \int d\vec{x}_r'' \tilde{W}(\vec{x}_o'', \vec{x}_r'') \tilde{H}_r(\vec{x}_r, \vec{x}_r'') \right|^2. \tag{14}$$

This equation takes a form identical to Eq. (12) except that $\tilde{H}_r$ is not conjugated. In this case, the corresponding effective object plane is located at a distance $(\lambda_o/\lambda_r) l_o$ from the left-hand side of the light source (the down-conversion crystal). From Fig. 2(b), we see that the CCD camera with the imaging lens works as if it were imaging a virtual image located at the effective object plane.

We can also see from Fig. 2 that nondegenerate-wavelength ghost imaging resembles paraxial refractive optics; the quantum setup is similar to imaging an object immersed in a positive refractive index material [10] whereas the classical setup is similar to imaging an object immersed in a negative refractive index material [15,16].

IV. RESOLUTION OF TWO-COLOR GHOST IMAGING

To study quantitatively the quality of the thermal ghost image, we make use of the Gaussian-Schell model [17] to describe the spatial coherence of the light leaving the SLMS. This model describes the Gaussian nature of the correlations generated by the random mask. We take the coherence function to be given by

$$W(\vec{x}_o', \vec{x}_r') = \exp\left(-\frac{\vec{x}_o'^2 + \vec{x}_r'^2}{4w^2} \right) \exp\left[-\frac{(\vec{x}_o' - \vec{x}_r')^2}{2\sigma_x^2} \right], \tag{15}$$

where w is the diameter of the laser beams illuminating the SLMS (or the nonlinear crystal for the quantum case) and σ_x determines the size of the spatial correlations of the two beams of light at the output plane of the SLMS. We consider the situation of λ_o and $\lambda_r < \sigma_x \ll w$ with $\lambda_a = 2\pi c/\Omega_a$.

According to Eq. (11), the propagated correlation function $\tilde{W}$ is given by

$$\tilde{W}(\vec{x}_o'', \vec{x}_r'') = \exp[i\alpha(\vec{x}_o''^2 - \vec{x}_r''^2)] \exp\left[-\frac{\vec{x}_o''^2 + \vec{x}_r''^2}{4\tilde{w}^2} \right] \times \exp\left[-\frac{(\vec{x}_o'' - \vec{x}_r'')^2}{2\tilde{\sigma}_x^2} \right], \tag{16}$$

where $\alpha \equiv (\pi/\lambda_o l_o)[1 + (2\pi w \sigma_x)^2/(\lambda_o l_o)^2]^{-1}$, $\tilde{\sigma}_x^2 \equiv \sigma_x^2 + (\lambda_o l_o)^2/(2\pi w)^2$, and $\tilde{w}^2 \equiv w^2 + (\lambda_o l_o)^2/(2\pi\sigma_x)^2$. To perform the integral in Eq. (12) more readily, we approximate the finite size of the imaging lens by replacing the step function $\theta(|\vec{x}| - D)$ in $L(\vec{x})$ with a Gaussian function of the form $\exp[-\vec{x}^2/(2D^2)]$. The power distribution $P(\vec{x}_r)$ of the ghost image thus takes the form

$$P(\vec{x}_r) = N \exp\left(-\frac{\vec{x}_r^2}{\Delta_{\mathrm{FOV}}^2} \right) \int d\vec{x}_o'' |O(\vec{x}_o'')|^2 \exp\left[-\frac{(\vec{x}_o'' - \vec{x}_r/m)^2}{\Delta_{\mathrm{PSF}}^2} \right]. \tag{17}$$

Here Δ_{PSF} is the width of the point-spread function that describes the resolution of the system as measured in object space. Also, Δ_{FOV} is the field of view as measured in image space and m is the magnification factor defined as the ratio of image height to object height, which is always negative in our system. The width of the point-spread function is given explicitly by

$$\frac{1}{\Delta_{\mathrm{PSF}}^2} = \mathrm{Re}\left[\left(\frac{2\pi}{\lambda_o l_o}\right)^2\left\{\frac{1}{\sigma_x^2} - \frac{2\pi i}{\lambda_o l_o} - \frac{1}{\sigma_x^4}\left[\frac{1}{\sigma_x^2} + \frac{2\pi i}{\lambda_r l_{r1}} + \left(\frac{2\pi}{\lambda_r l_{r1}}\right)^2\left(\frac{1}{D^2} + \frac{2\pi i}{\lambda_r l_r}\right)^{-1}\right]^{-1}\right\}^{-1}\right], \tag{18}$$

where $l_r^{-1} \equiv l_{r1}^{-1} + l_{r2}^{-1} - f^{-1}$.

The ghost image attains its highest resolution when Δ_{PSF} is minimum. We find by straightforward differentiation that Δ_{PSF} is minimum (for fixed l_{r1}) when the position of the imaging lens satisfies the thin-lens equation

$$\frac{1 + (\lambda_r l_{r1}\lambda_o l_o)/(4\pi^2 w^2 D^2)}{l_{r1} - (\lambda_o/\lambda_r) l_o} + \frac{1}{l_{r2}} - \frac{1}{f} = 0, \tag{19}$$

where we have assumed that $D \gg \sigma_x$. Note that the contribution $(\lambda_r l_{r1}\lambda_o l_o)/(4\pi^2 w^2 D^2)$ to the numerator of the first term of this expression is absent in previous treatments [4,18].

The minimum width of the point-spread function referred to object space [that is, normalized by the magnification $m \approx \lambda_r l_{r2}/(\lambda_o l_o - \lambda_r l_{r1})$] is then given by

$$\Delta_{\mathrm{PSF}} = \sqrt{\sigma_x^2 + \left(\frac{\lambda_o l_o}{2\pi w}\right)^2 + \frac{(\lambda_r l_{r1} - \lambda_o l_o)^2}{(\lambda_r l_{r1}/w)^2 + (2\pi D)^2}}. \tag{20}$$

It is noted that the sum of the first two terms of Δ_{PSF} gives $\tilde{\sigma}_x^2$, that is, the spatial correlation distance as measured at the effective object plane. The third term is due to the finite size of the imaging lens aperture. It depends on the effective distance $l_{r1} - (\lambda_o/\lambda_r) l_o$ between the object and the imaging lens but not on the focal length f and the distance l_{r2} between the lens and the CCD. It should be noted that Δ_{PSF} attains its minimum value when $\lambda_r l_{r1} = \lambda_o l_o$. In this case, as seen in Fig. 2(a), the imaging lens is located at the effective object plane, and the lens is not required in order to obtain a ghost image. This result also implies that the lensless version of the thermal ghost imaging [5,11,12] always gives the best resolution. Alternatively, when a lens is used but the lens diameter is sufficiently large such that diffraction effects become negligible (that is, for $D \to \infty$), $\tilde{H}_r(\vec{x}_r, \vec{x}_r'')$ reduces to $\delta(\vec{x}_r - \vec{x}_r'')$ so that Eq. (12) gives results equivalent to those of a lensless thermal ghost imaging configuration.

Equation (20) is plotted in Fig. 3(a) as a function of λ_r for various λ_o with l_o and l_{r1} fixed. It is seen that the width of the point-spread function Δ_{PSF} attains its smallest value when $\lambda_o/\lambda_r = l_{r1}/l_o$, as discussed above. It also depends more strongly on λ_o than λ_r, especially near its minimum values. The corresponding plot of Δ_{PSF} for the quantum case is shown in Fig. 3(b), which is obtained by inverting the sign of λ_o in Eq. (20). We note that in the same configuration, the Δ_{PSF} for thermal ghost imaging is always smaller than that for the quantum case. This result is due to the fact that the third term of Eq. (20) for the quantum case is always larger than that for the thermal case. This term can nevertheless be made arbitrarily small, for both the quantum and thermal cases, when the imaging lens is sufficiently large. In this limit of a large lens aperture, the resolution of the ghost image depends solely on the wavelength λ_o used to illuminate the object. It is also apparent from Fig. 3 that for the thermal case, as λ_r increases the plots of Δ_{PSF} versus λ_o cross

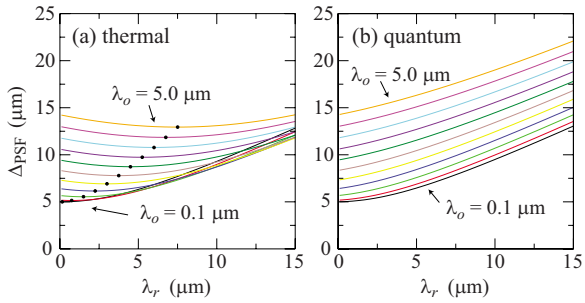

FIG. 3. (Color online) (a) Width of the point-spread function Δ_{PSF} as a function of λ_r for (from bottom to top) λ_o=0.1, 0.5, 1.0, 1.5, 2.0, 2.5, 3.0, 3.5, 4.0, 4.5, and 5.0 μm. Parameters used are σ_x=5 μm, w=10 mm, D=20 mm, l_{r1}=100 mm, and l_o =150 mm. The dots denote the cases with $\lambda_r = (l_o/l_{r1})\lambda_o = 1.5\lambda_o$, in which case Δ_{PSF} attains the smallest value for a given λ_o. (b) The corresponding plot of Δ_{PSF} for nondegenerate-wavelength quantum ghost imaging.

each other, whereas for the quantum case they never cross. Finally, the resolutions for the thermal and quantum ghost imaging are the same when λ_o or λ_r tends to zero.

When w is large enough so that diffraction from the source plane to the object plane is negligible and when the lens condition given by Eq. (19) is satisfied, the width of point-spread function normalized by magnification given in Eq. (20) can be rewritten as

$$\Delta_{\mathrm{PSF}} = \sqrt{\sigma_x^2 + \left[\left(\frac{\lambda_r}{2\pi}\right)\left(\frac{1-m}{m}\right)F\right]^2}, \tag{21}$$

where m is the magnification and $F \equiv f/D$ is the f-number of the imaging lens. This result is valid for both quantum and thermal ghost images. In this limit, we note that if we fix the magnification, instead of the object and lens distances from the source plane, we find identical resolution for both thermal and quantum ghost images.

The result in Eq. (21) is in agreement with that of Rubin and Shih [10]. In their calculation they only considered the limit where w is large and σ_x is negligible. They find that the smallest resolvable length scale (normalized by the magnification) for a nondegenerate-wavelength quantum ghost imaging system is, using our notation,

$$a_{\min} = 0.61\frac{\lambda_r l_{r1} + \lambda_o l_o}{D} = 0.61\left|\frac{1-m}{m}\right|F, \tag{22}$$

where, in rewriting their expression in terms of F, we inverted the sign of λ_o as required for a quantum ghost imaging system (see Sec. II). In this expression, the numerical factor $1/(2\pi)$ in Eq. (21) is replaced by 0.61. These different numerical factors arise from the different definitions of resolution as well as the Gaussian approximations made in our calculation. Although this result gives the limiting resolution of an ideal ghost imaging system, Eq. (20) is more general, since in typical situations the effects of σ_x and w are not negligible.

V. DISCUSSIONS AND CONCLUSION

Although it may seem surprising that classical states, which cannot violate any EPR uncertainty relation, image with better resolution than do entangled states for fixed object and lens distances, there is no contradiction, as also pointed out in Refs. [9,19]. Here Eq. (20) shows explicitly the parameters that govern the resolution of the ghost image and explains the sources of the contributions. In fact, using the unfolded diagrams and from the thin-lens equation [Eq. (19)], we can see that the object has a shorter effective distance to the imaging lens in the reference arm in the thermal setup than in the quantum setup due to the conjugation of the beams [see Fig. 2(b)]. As a result, the thermal ghost imaging setup has a larger effective numerical aperture and produces images with better resolution.

One may understand nondegenerate-wavelength thermal ghost imaging by realizing that there is always a plane (effective object plane) in the reference arm that has the same spatial intensity pattern of the light as that on the object in the object arm. This is similar to degenerate-wavelength ghost imaging, in which the speckles patterns are always the same on every two planes in the object and reference arms that are equidistant from the ground glass plate. For nondegenerate-wavelength thermal ghost imaging, this effective object plane is located at a distance from the SLMS scaled by the ratio of the wavelengths of light in the object and reference arms. That is, both the signal and reference waves experience the same degree of diffraction in propagation from the SLMS.

In conclusion, we have shown that nondegenerate-wavelength ghost imaging with thermal light is not only possible but can also give better image resolution than quantum ghost imaging using entangled light. Moreover, there is no fundamental limit to the extent to which the wavelengths used in the object and reference arms can differ. This result leads to the remarkable consequence that it is possible to obtain a high-quality image of an object at a desired wavelength even if there are no imaging detectors that operate at this wavelength. In addition, we found that for both thermal and quantum ghost imaging, the resolution is limited primarily by the strength of the spatial correlation of the light beams, determined by σ_x, and depends more strongly on the wavelength of the light illuminating the object than on that of the reference arm. Finally, we remark that although thermal ghost imaging can provide higher resolution, it is well known that it tends to produce images of much lower contrast than does quantum ghost imaging, especially for complex objects [3,20,21].

ACKNOWLEDGMENTS

The authors would like to thank Claudio Parazzoli, Barbara Capron, Jonathan Dowling, and Jeffrey Shapiro for helpful discussions. This research was supported by the U.S. Army Research Office under a MURI grant and the Boeing Co.

[1] T. B. Pittman, Y. H. Shih, D. V. Strekalov, and A. V. Sergienko, Phys. Rev. A **52**, R3429 (1995).
[2] R. S. Bennink, S. J. Bentley, and R. W. Boyd, Phys. Rev. Lett. **89**, 113601 (2002).
[3] A. Gatti, E. Brambilla, M. Bache, and L. A. Lugiato, Phys. Rev. Lett. **93**, 093602 (2004); Phys. Rev. A **70**, 013802 (2004).
[4] A. Valencia, G. Scarcelli, M. D'Angelo, and Y. H. Shih, Phys. Rev. Lett. **94**, 063601 (2005).
[5] G. Scarcelli, V. Berardi, and Y. H. Shih, Phys. Rev. Lett. **96**, 063602 (2006). The argument used in this paper to explain the quantum nature of thermal ghost imaging is debatable. See A. Gatti, M. Bondani, L. A. Lugiato, M. G. A. Paris, and C. Fabre, *ibid.* **98**, 039301 (2007).
[6] B. I. Erkmen and J. H. Shapiro, Phys. Rev. A **77**, 043809 (2008); **78**, 023835 (2008).
[7] I. P. Degiovanni, M. Bondani, E. Puddu, A. Andreoni, and M. G. A. Paris, Phys. Rev. A **76**, 062309 (2007).
[8] T. B. Pittman, D. V. Strekalov, D. N. Klyshko, M. H. Rubin, A. V. Sergienko, and Y. H. Shih, Phys. Rev. A **53**, 2804 (1996).
[9] M. D'Angelo, A. Valencia, M. H. Rubin, and Y. H. Shih, Phys. Rev. A **72**, 013810 (2005).
[10] M. H. Rubin and Y. Shih, Phys. Rev. A **78**, 033836 (2008).
[11] J. Cheng and S. Han, Phys. Rev. Lett. **92**, 093903 (2004).
[12] G. Scarcelli, V. Berardi, and Y. H. Shih, Appl. Phys. Lett. **88**, 061106 (2006).
[13] B. E. A. Saleh, A. F. Abouraddy, A. V. Sergienko, and M. C. Teich, Phys. Rev. A **62**, 043816 (2000).
[14] D.-Z. Cao, J. Xiong, and K. Wang, Phys. Rev. A **71**, 013801 (2005).
[15] V. G. Veselago, Sov. Phys. Usp. **10**, 509 (1968).
[16] J. B. Pendry, Phys. Rev. Lett. **85**, 3966 (2000).
[17] L. Mandel and E. Wolf, *Optical Coherence and Quantum Optics* (Cambridge University Press, Cambridge, England, 1995).
[18] M. D'Angelo, Y.-H. Kim, S. P. Kulik, and Y. H. Shih, Phys. Rev. Lett. **92**, 233601 (2004).
[19] F. Ferri, D. Magatti, A. Gatti, M. Bache, E. Brambilla, and L. A. Lugiato, Phys. Rev. Lett. **94**, 183602 (2005).
[20] Y. Cai and S.-Y. Zhu, Phys. Rev. E **71**, 056607 (2005).
[21] L. Basano and P. Ottonello, Opt. Express **15**, 12386 (2007).